Journal of Vacuum Science & Technology A

Deposition of Sputtered NiO as a p-type Layer for Heterojunction Diodes with Ga_2O_3

Running title: Deposition of Sputtered NiO

Running Authors: Li et al.

Jian-Sian Li[1], Xinyi Xia[1], Chao-Ching Chiang[1], David C. Hays[2], Brent P. Gila[2,3], Valentin Craciun[4,5], Fan Ren[1] and S.J. Pearton [1,a)]

[1] Department of Chemical Engineering, University of Florida, Gainesville, FL 32606 USA
[2] Nanoscale Research Facility, University of Florida, Gainesville FL 32611 USA
[3] Department of Materials Science and Engineering, University of Florida, Gainesville, FL 32606 USA
[4] National Institute for Lasers, Plasma and Radiation Physics, 077125 Magurele, Romania
[5] Extreme Light Infrastructure for Nuclear Physics, IFIN-HH, 077125 Magurele, Romania

[a)] Electronic mail: spear@mse.ufl.edu

The characteristics of sputtered NiO for use in pn heterojunctions with Ga_2O_3 were investigated as a function of sputtering parameters and post-deposition annealing temperature. The Oxygen/ Nickel and Ni_2O_3/NiO ratios, as well as the bandgap and resistivity, increased as a function of O_2/Ar gas flow ratio. For example, bandgap increased from 3.7 to 3.9 eV and the resistivity increased from 0.1 to 2.9 Ω.cm for O_2/Ar ratio increasing from 1/30 to 1/3. By sharp contrast, the bandgap and Ni_2O_3/NiO ratio decreased monotonically with post-deposition annealing temperatures up to 600°C, but the density of the films increased due to a higher fraction of NiO being present. Hydrogen is readily incorporated into the NiO during exposure to plasmas, as delineated by Secondary Ion Mass Spectrometry measurements on deuterated films. The band alignments of the NiO films were type II- staggered gap with both α- and β-Ga_2O_3. The breakdown voltage of NiO/β-Ga_2O_3 heterojunction rectifiers was also a strong function of O_2/Ar flow ratio during deposition, with values of 1350 V for 1/3 and 830V for 1/30.

I. INTRODUCTION

NiO is a well-established p-type oxide [1] which has found renewed application as a component of p-n heterojunctions with β-Ga_2O_3 in high power rectifiers [2-17]. This provides a solution to the lack of a robust p-type doping capability in Ga_2O_3 [3], allowing the demonstration of high breakdown voltages and forward conduction currents with NiO/Ga_2O_3 heterojunction rectifiers [2-17]. The NiO may also be used as edge termination or p-type guard rings in such devices [10], but clearly the design parameters have not been optimized in terms of thickness, resistivity, stoichiometry and other parameters for the NiO used in these applications [4-17].

There have been many studies of the properties of NiO deposited by a number of methods [18-32], including e- beam evaporation [23], reactive sputtering [24] or atomic layer deposition [26], but few specifically related to the thin layers needed in NiO/Ga_2O_3 devices, which must also typically undergo annealing treatments during device processing. It is well-established that the NiO bandgap varies from ~3.6-4 eV, depending on deposition conditions and that the p-type conductivity is a strong function of the O_2 partial pressure during deposition [18-32].

In this work, we systematically vary the O_2/ Ar ratio during multi-source NiO target magneton sputtering and also perform post-deposition annealing up to 600°C. The composition, bandgap, density and surface roughness of the NiO films were measured for all these conditions and the effect of O_2/Ar gas flow ratio on the breakdown voltage of NiO/β-Ga_2O_3 heterojunction rectifiers was quantified. We also investigated the ease of incorporation of hydrogen during simulated plasma enhanced chemical vapor deposition processes. This work provides a framework for optimizing the incorporation of NiO into Ga_2O_3 power devices.

Journal of Vacuum Science & Technology A

II. EXPERIMENTAL

The deposition was performed in a Kurt J. Lesker Multi-Source Sputter System using dual NiO targets. The 13.56 MHz rf power during deposition was 150W at a pressure of 3mTorr, producing a deposition rate of 12 nm/min (2 Å/sec). The gas flow ratios of O_2/Ar were 1/3, 1/7, 1/10 or 1/30. The deposition temperature was nominally room temperature and was < 100°C. All of the NiO films were polycrystalline, as determined by x-ray diffraction. The NiO was deposited on to quartz slides for calibration of sputter rate, resistivity, composition, density and morphology and also on to β-Ga_2O_3 structures consisting of 10 μm epi layers with doping $3x10^{16}$ cm^{-3} deposited by Hydride Vapor Phase Epitaxy onto a (001) oriented n^+ Sn-doped Ga_2O_3 substrates for fabrication of heterojunction rectifiers whose processing sequence has been described in detail elsewhere [10]. The current-voltage (I-V) characteristics of these devices were recorded with a Tektronix 370-A curve tracer, 371-B curve tracer and Agilent 4156C parameter analyzer. The reverse breakdown voltage was defined as the bias for a reverse current reaching 0.1 $A.cm^2$. Hall measurements were used to obtain carrier mobilities. In a few cases, we also deposited the NiO on to 1μm thick α-polytype Ga_2O_3 layers grown on sapphire substrates in order to compare band alignment of NiO on both α- and β-polytype samples before and after annealing up to 600°C under O_2 ambient. Finally, some of the NiO films were exposed to ^2H plasmas at 200°C for 30 min and then subsequently annealed at 300°C to simulate typical PECVD processes and contact annealing steps. The deuterium profiles in the samples were measured by Secondary Ion Mass Spectrometry (SIMS).

The compositional analysis was done by measuring the ratio of ratio of O/Ni transitions in X-Ray Photoelectron Spectroscopy (XPS) spectra. For the Ni_2O_3/ NiO phases, we were not able to separate the peaks of Ni^{2+} and Ni^{3+} because they are too close in energy. The XPS system was a Physical Instruments ULVAC PHI, with an Al x-ray source (energy 1486.6 eV, source power 300W), analysis size of 100 μm diameter, a take-off angle of 50° and acceptance angle of ±7 degrees. The electron pass energy was 23.5 eV for high-resolution scans. The bandgap was extracted from Tauc plots of absorbance obtained using UV-Vis (Perkin-Elmer Lambda 800 UV/Vis) spectrometer). The film density and surface roughness were obtained from X-Ray Reflectometry (XRR) measurements using an XRR measurements have been performed on the PANalytical Empyrean ω/2Θ diffractometer system. The acquired spectra were modeled with the freeware GenX (GenX) software package. Features of the XRR spectrum such as the critical angle, periodicity of oscillation and their amplitude are directly related to the density, thickness and roughness of the actual structure. The ratio of NiO/Ni_2O_3 as obtained from X-Ray Diffraction (XRD) measurements. The XRD analysis was performed using a Brucker D8 Advance diffractometer. The crystalline structure of the NiO thin films was established by applying the standard XRD technique using Cu Kα radiation (λ = 1.55418 Å) in the range of 2θ = 25–80 degrees. Band alignments were also determined by XPS.

III. RESULTS AND DISCUSSION

Figure 1 shows the XPS spectrum of a typical NiO film. The different valence transitions for Ni present show the film is a mixture of NiO and Ni_2O_3. There are two different components of the oxygen peak in the composition calculation, namely 529.3eV

as the main oxygen peak and 531eV which is associated with oxygen next to a Ni vacancy, which can be used to calculate the oxygen concentration in the material. There are also multiple components within the main Ni peak [34].

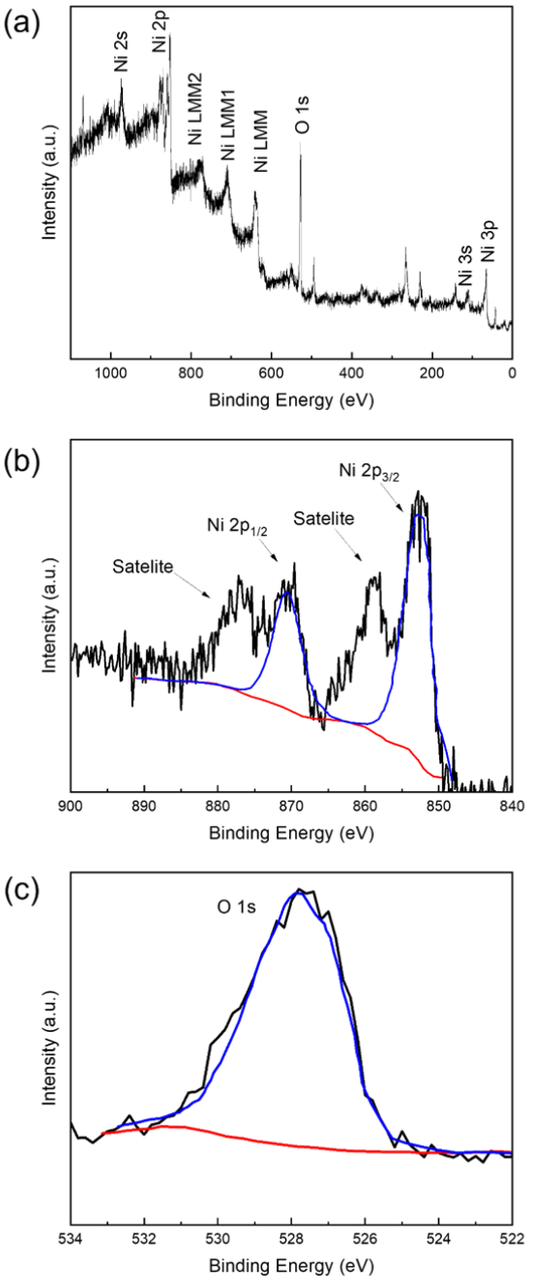

Fig. 1.(a) XPS survey spectrum of NiO film (b) expanded view of Ni 2p peaks region (c) expanded view of O 1s peak region

Figure 2 (a) shows the oxygen/ nickel ratio and Ni_2O_3/NiO as a function of O_2/Ar gas flow ratio. NiO films deposited at a higher ratio of oxygen gas flow have higher oxygen content related to the higher proportion of Ni_2O_3. Figure 2 (b) shows the energy bandgap and resistivity of NiO films as a function of oxygen/argon flow ratio. The stoichiometry of NiO is dependent upon the deposition parameters. The bandgap was obtained from the Tauc plot, where we obtained better fitting to the absorbance data assuming a square power dependence in the plot of $(\alpha hv)^2$ as a function of the photon energy hv. This suggests the bandgap is direct [(1)]. In these relations, α and hv are the absorption coefficient and photon energy, respectively. With a higher ratio of oxygen gas flow, the Eg and the resistivity both increase. The bandgap trend is in general agreement with past reports where the films were deposited by sputtering at elevated temperature (200 °C) [(22)], but the resistivity in that case strongly decreased with increasing oxygen content due to an increase in carrier concentration [(22)]. The increase in hole concentration was ascribed to nickel vacancies and oxygen interstitials. However, in our films deposited near room temperature, the increasing oxygen content leads to a relatively small increase in resistivity, with no increase in oxygen interstitials and nickel vacancies. The hole concentration was $2x10^{18}$ cm^{-3} for 1/3 O_2/Ar gas ratio and $2x10^{19}$ cm^{-3} for 1/30 gas ratio, with a mobility of <1 $cm^2 V^{-1} s^{-1}$ in all cases. Table 1 summarizes the changes in bandgap and film composition as a function of O_2/Ar ratio during sputtering.

The stability of NiO film properties during post-deposition annealing was measured, since this is relevant to device processing sequences where Ohmic contacts have to be

annealed and dielectric films might be deposited for a variety of purposes, including surface passivation or encapsulation. Figure 3 shows the energy bandgap and Ni_2O_3/NiO ratio of NiO films as a function of post-deposition annealing temperatures. With increasing annealing temperature, the Eg decreases and more oxygen escapes from the film, corresponding to a decrease in the Ni_2O_3/NiO ratio.

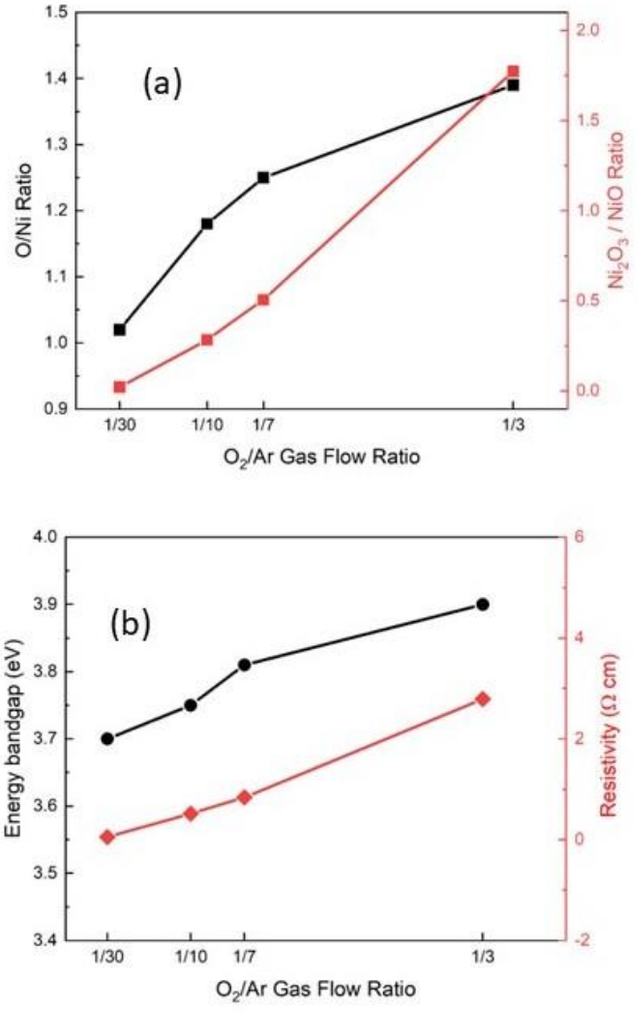

Fig 2. (a) Oxygen/ nickel ratio and Ni_2O_3/NiO ratio and (b) energy bandgap and resistivity as a function of O_2/Ar gas flow ratio.

Table 1. Composition and bandgap data for films as a function of O_2/Ar flow rate during sputtering.

O_2/Ar flow rate ratio	1/3	1/7	1/10	1/30
O (atomic %)	58.2	55.6	54.1	50.5
Ni (atomic %)	41.8	44.4	45.9	49.5
O/Ni	1.39	1.25	1.18	1.02
Ni_2O_3/NiO	1.77	0.51	0.28	0.02
E_g (eV)	3.90	3.81	3.75	3.70

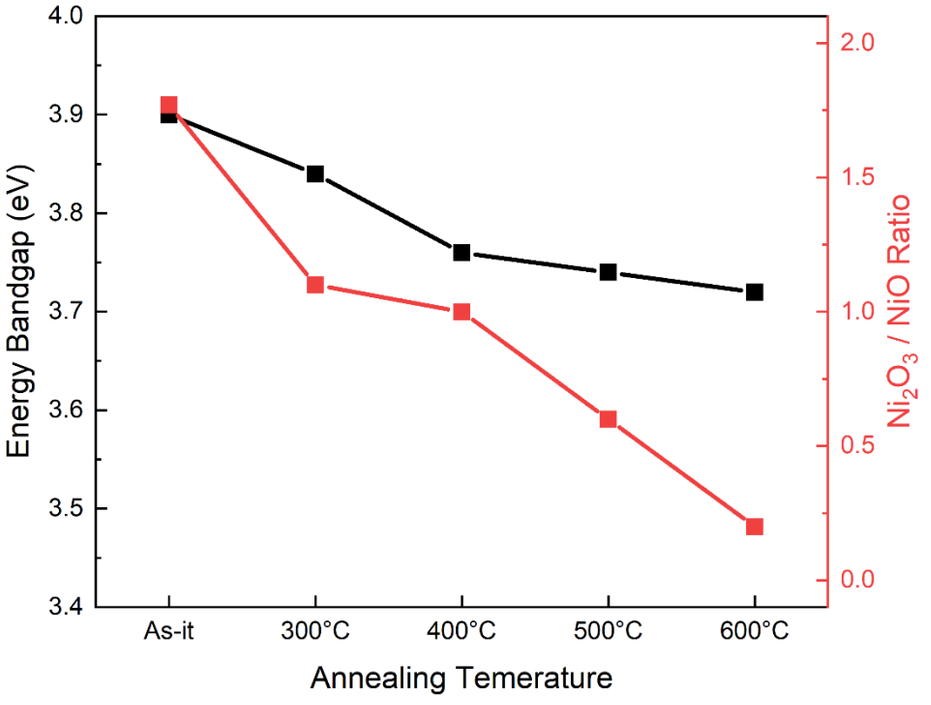

Fig. 3. Energy bandgap and Ni_2O_3/NiO ratio in NiO films as a function of annealing temperatures.

Another issue of interest during such simulations for process steps is the diffusion of hydrogen, which might occur during annealing in forming gas or during plasma enhanced chemical vapor deposition of dielectrics. In general, hydrogen is an unavoidable impurity in oxide semiconductor films deposited by sputtering, due to incorporation through reactions with residual gas species, H_2O and H_2, within the vacuum chamber [35]. NiO samples grown with 1/3 O_2/Ar gas ratio were treated in D_2-plasmas for 30 min at a nominal temperature of 200 °C and were characterized with Secondary Ion Mass Spectrometry (SIMS) at EAG Laboratories before and after subsequent annealing at 300°C. Detection limits for SIMS for D were 3 x 10^{15} cm^{-3}. Figure 4 (a) shows SIMS profiles of the ^2H in the film after plasma exposure, with a very high concentration of deuterium incorporated. Subsequent annealing lowered this by approximately a factor of 5, as shown in Figure 4(b), but a high concentration remains (~10^{20} cm^{-3}). Plots of the deuterium profiles before and after annealing are shown in Figure 4 (c).Since hydrogen is an important n-type dopant in a variety of conducting oxides [36, 37], it could have substantial influence on the conductivity of the NiO and also it is known to influence the surface properties of Ga_2O_3 [38, 39]. The resistivity of the sample changed from 2.9 Ω. cm to 1.6 Ω. cm after the plasm treatment.

In a similar vein, the band offset of NiO on Ga_2O_3 is of interest to determine its ability as a hole injector. We have reported [17, 40] that this band alignment is type II staggered gap for NiO on both β-Ga_2O_3 [17] and GaN [40]. The band alignments were determined from the standard X-Ray Photoelectron Spectroscopy (XPS) method [41-43]. We also measured this for NiO on the α-polytype of Ga_2O_3 to assess the generality of this trend in band alignment. Figure 5 shows band alignments for (a) NiO/ β-Ga_2O_3 and (b)

NiO/α-Ga_2O_3 both as-deposited and different annealing temperatures and the same trends are seen for both polytypes. The band alignment remains as staggered gap across the entire annealing range.

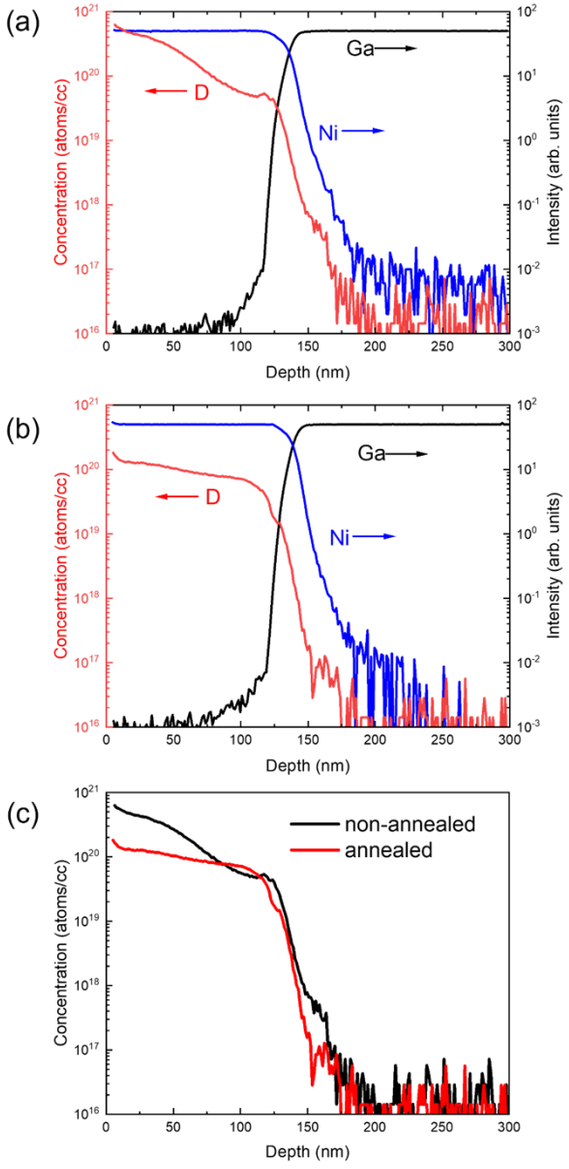

Fig. 4. SIMS profiles of deuterium in ^2H plasma exposed NiO at 200°C (a) as-exposed and (b) after subsequent annealing at 300°C.(c) shows a detailed comparison of the deuterium profiles before and after annealing.

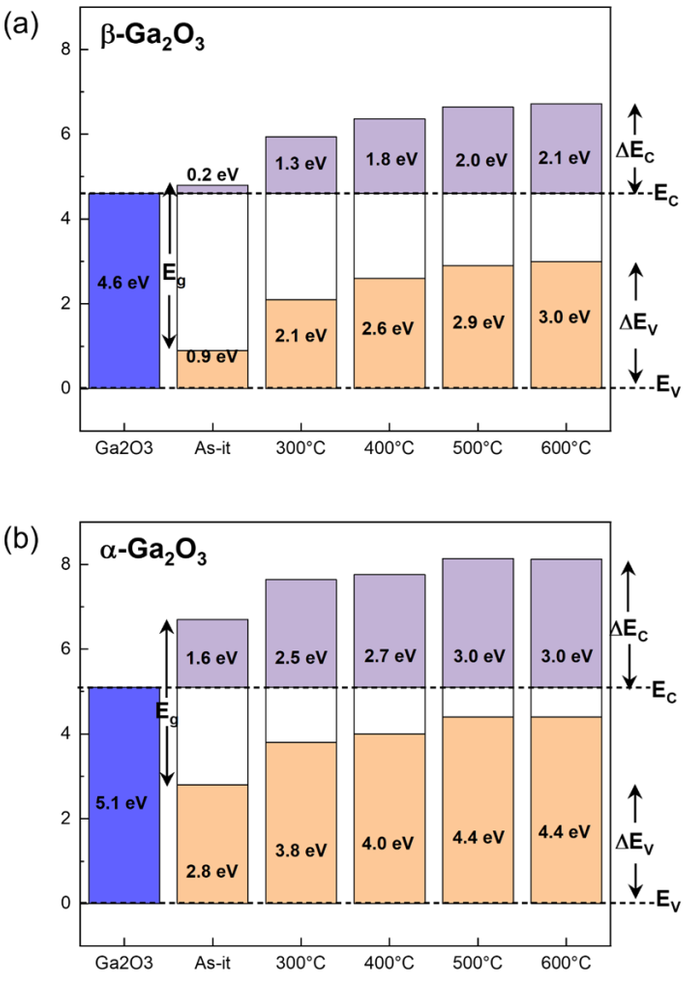

Fig 5. Band alignments for (a) NiO/ β-Ga_2O_3 and (b) NiO/α-Ga_2O_3 for as-deposited and different annealing temperatures.

Figure 6 (a) shows that with the increase of annealing temperature, the density of the films obtained from XRR increases due to more NiO being formed relative to Ni_2O_3. The density of the former is 6.67 g/cm^3, while the density of Ni_2O_3 is 4.84 g/cm^3. The roughness of the films also increases with increasing annealing temperatures. As shown in the XRD spectra of Figure 6 (b), the Ni_2O_3 peak decreases with higher annealing

temperature so that the amount of Ni_2O_3 decreases with higher annealing temperature, consistent with the decrease of film density. Table 2 summarizes the annealing temperature induced changes in bandgap, resistivity, Ni_2O_3/NiO ratio, density, surface roughness and band offsets. The increase of resistivity with annealing temperature is speculated may be due to an increased concentration of oxygen vacancies.

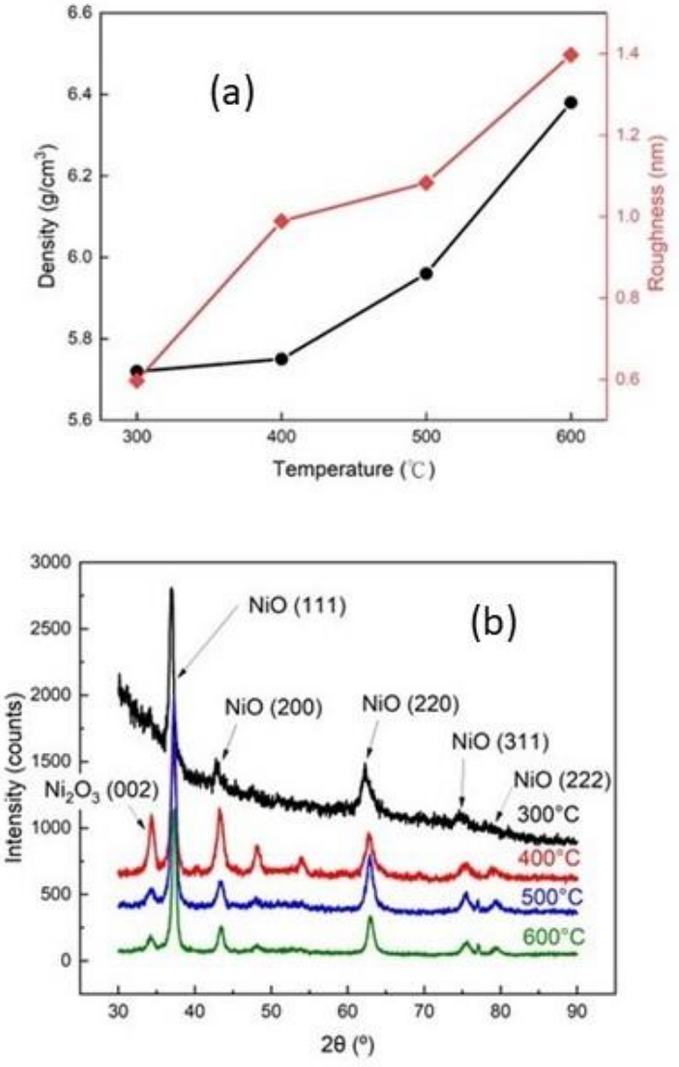

Fig. 6. (a) Film density and surface roughness and (b) XRD spectra as a function of different annealing temperatures.

Table 2. Composition, resistivity, band offsets, density and RMS roughness data for films as a function of post deposition annealing temperature.

Temperature (°C)	As-Dep	300	400	500	600
Ni_2O_3/NiO	1.77	1.08	1.01	0.63	0.19
Resistivity (Ω·cm)	2.79	5.6	> 10	> 10	> 10
E_g (eV)	3.90	3.84	3.76	3.74	3.72
ΔE_c (eV) (β-Ga_2O_3)	0.2	1.34	1.76	2.04	2.12
ΔE_v (eV) (β-Ga_2O_3)	0.9	2.1	2.6	2.9	3
ΔE_c (eV) (α-Ga_2O_3)	1.6	2.54	2.66	3.04	3.02
ΔE_v (eV) (α-Ga_2O_3)	2.8	3.8	4	4.4	4.4
Density (g/cm^3)	5.50	5.72	5.75	5.96	6.38
Roughness (nm)	-	0.597	1.083	0.989	1.397

To determine the effect of sputtering conditions on the performance of NiO/Ga_2O_3 rectifiers, structures with a fixed NiO thickness of 240nm were fabricated, as shown in the schematic of Figure 7(a). With a higher ratio of oxygen gas flow, on-state resistance R_{on} and Vbi of the diode increased when O_2/Ar ratio was decreased, as shown in Figure 7(b). Concurrently, the turn on voltage V_{on} also decreased, as shown in Figure 7 (c). The ideality factor of the rectifiers was 2.7, indicating more than simply thermionic emission present. There was no systematic difference in barrier heights determined by I-V and C-V, indicating a low degree of interface inhomogeneity [(44)]. The V_{on} is calculated from the slope of the forward I-V curves. This is due to the lower resistivity of the film under these conditions. Correspondingly, the on/off ratio and the breakdown volage V_B increased because of lower conductivity at high O_2/Ar ratio, as shown in Figure 8(a) and (b), respectively. This shows the strong influence the deposition parameters of the NiO have

on the device performance of NiO/Ga_2O_3 rectifiers. The breakdown doesn't occur catastrophically, as defined by breakdown criteria of current reaching 0.1 mA/cm^2. For 200 µm diameter rectifiers, the reverse recovery time of ~21 ns was independent of temperature, with the I_{rr} monotonically increasing from 15.1 mA at 25°C to 25.6 mA at 250°C [45].

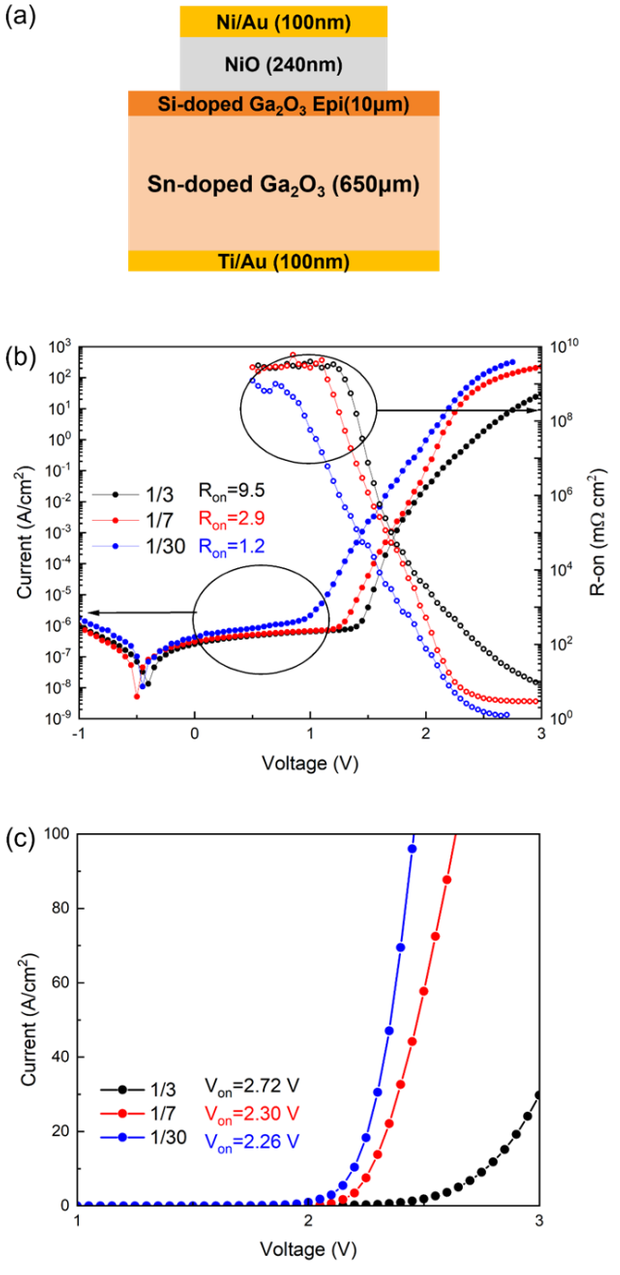

Fig 7. (a) Schematic of device structure (b) Forward current density and on-state resistance and (c) Forward turn-on voltage as a function of O_2/Ar gas flow ratio during deposition

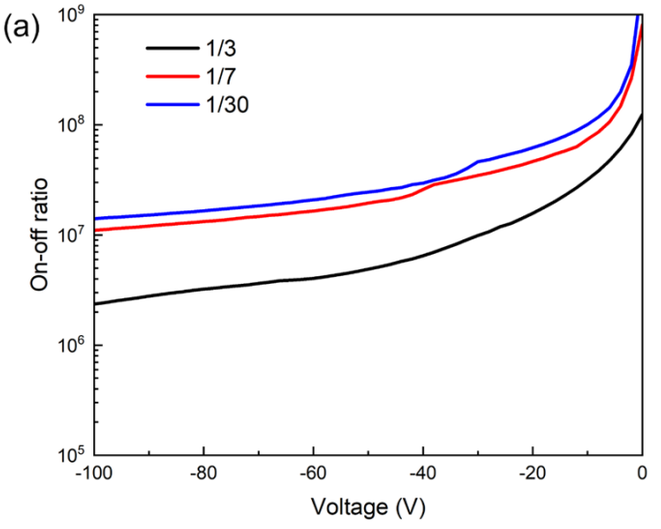

Fig. 8. (a) On-off ratio (b) Reverse I-V characteristics and associated breakdown voltages as a function of O_2/Ar gas flow ratio during deposition.

IV. SUMMARY AND CONCLUSIONS

The properties of thin NiO films deposited by magnetron sputtering and intended for use in heterojunction devices with Ga_2O_3 were examined as a function of deposition parameters and post-deposition annealing temperature to understand the effect of these parameters on device performance of NiO/β-Ga_2O_3 rectifiers. The bandgap, resistivity, density and composition are all affected by O_2/Ar ratio during deposition. Post-deposition annealing up to 600°C also changes the film properties in a controlled fashion. High amounts of hydrogen are included during exposure to simulated PECVD conditions. The device performance of heterojunction rectifiers is optimized at lower O_2 relative flow rates, due to a lower resistivity in the NiO films. With recent breakthroughs like use of $(Al_xGa_{1-x})_2O_3$ to enhance the bandgap in rectifiers [46], there are now more options available to enhance the ;performance of these devices.

ACKNOWLEDGMENTS

The authors would like to thank the Research Service Center (RSC) staff at the University of Florida for their help in the fabrication and characterization of these materials. The work at UF was performed as part of Interaction of Ionizing Radiation with Matter University Research Alliance (IIRM-URA*)*, sponsored by the Department of the Defense, Defense Threat Reduction Agency under award HDTRA1-20-2-0002. The content of the information does not necessarily reflect the position or the policy of the federal government, and no official endorsement should be inferred. The work at UF was also supported by NSF DMR 1856662 (James Edgar). The work in Romania was supported by the Romanian Ministry of Education and Research, under the Romanian National Nuclear Program LAPLAS VI (contract

n. 16N/2019), ELI-RO_2020_12, and Postdoctoral Project PD 145/2020.

AUTHOR DECLARATIONS

Conflicts of Interest

The authors have no conflicts to disclose.

DATA AVAILABILITY

The data that supports the findings of this study are available within the article

REFERENCES

[1]D. J.A. Spencer, A.L. Mock, A.G. Jacobs, M. Schubert, Y. Zhang and M.J. Tadjer, Appl. Phys. Rev. 9, 011315 (2022).

[2]F. Vera, R. Schrebler, E. Munoz, C. Suarez, P. Cury, H. Gomez, R. Cordova, R. E. Marotti, and E. A. Dalchiele, Thin Solid Films 490, 182 (2005).

[3]S. Lany, J. Osorio-Guillen, A. Zunger, Phys. Rev. B Condens. Matter 75, 1 (2007).

[4]Y. M. Lu, W. S. Hwang, and J. S. Yang, Surf. Coat. Technol. 155, 231 (2002).

[5]M. Tyagi, M. Tomar, and V. Gupta, IEEE Electr. Device L. 34, 81 (2013).

[6]Jincheng Zhang, Pengfei Dong, Kui Dang, Yanni Zhang, Qinglong Yan, Hu Xiang, Jie Su, Zhihong Liu, Mengwei Si, Jiacheng Gao, Moufu Kong, Hong Zhou and Yue Hao, Nat Commun 13, 3900 (2022).

[7]Yuangang Wang, Hehe Gong, Yuanjie Lv , Xingchang Fu, Shaobo Dun, Tingting Han, Hongyu Liu, Xingye Zhou, Shixiong Liang, Jiandong Ye, Rong Zhang, Aimin Bu, Shujun Cai and Zhihong Feng, IEEE T. Power Electr. 37, 3743 (2022).

[8]Hong Zhou, Shifan Zeng, Jincheng Zhang, Zhihong Liu, Qian Feng, Shengrui Xu, Jinfeng Zhang and Yue Hao, Crystals 11, 1186 (2021).

[9]A. Takatsuka, K. Sasaki, D. Wakimoto, Q. T. Yhieu, Y. Koishikawa, J.Arima, J. Hirabayashi, D. Inokuchi, Y. Fukumitsu, A. Kuramata, S. Yamakoshi, "Fast Recovery Performance of β-Ga_2O_3 Trench MOS Schottky Barrier Diodes", in Proc. of the 76th Device Research Conf., IEEE, pp. 1–2, USA 2018.

[10]Jian-Sian Li, Chao-Ching Chiang, Xinyi Xia, Timothy Jinsoo Yoo, Fan Ren, Honggyu Kim and S.J. Pearton, Appl. Phys. Lett. 121, 042105 (2022).

[11]Hehe Gong, Feng Zhou, Weizong Xu, Xinxin Yu, Yang Xu, Yi Yang, Fang-fang Ren, Shulin Gu, Youdou Zheng, Rong Zhang, Hai Lu and Jiandong Ye, IEEE T. Power Electr., 36, 12213 (2021).

[12]Y. Lv, Y. Wang, X. Fu , Shaobo Dun, Z. Sun, Hongyu Liu, X. Zhou, X. Song, K. Dang, S. Liang, J. Zhang, H. Zhou, Z. Feng, S. Cai and Yue Hao, IEEE T. Power Electr. 36, 6179 (2021).

[13]Chenlu Wang, Hehe Gong, Weina Lei, Y. Cai, Z. Hu, Shengrui Xu, Zhihong Liu , Qian Feng , Hong Zhou, Jiandong Ye, Jincheng Zhang, Rong Zhang, and Yue Hao, IEEE Electr. Dev. L, 42, 485 (2021).

[14]S. Roy, A. Bhattacharyya, P. Ranga, H. Splawn, J. Leach, and S. Krishnamoorthy, IEEE Electr. Dev L., 42, 1540 (2021).

[15]Qinglong Yan, Hehe Gong, Jincheng Zhang, Jiandong Ye, Hong Zhou, Zhihong Liu, Shengrui Xu, Chenlu Wang, Zhuangzhuang Hu, Qian Feng, Jing Ning, Chunfu Zhang, Peijun Ma, Rong Zhang, and Yue Hao, Appl. Phys. Lett. 118, 122102 (2021).

[16]H. H. Gong, X. H. Chen, Y. Xu, F.-F. Ren, S. L. Gu and J. D. Ye, Appl. Phys. Lett., 117, 022104 (2020).

[17]Xinyi Xia, Jian Sian Li, Chao Ching Chiang, Timothy Jinsoo Yoo, Fan Ren, Honggyu Kim and S.J. Pearton, J. Phys. D 55, 385105 (2022).

[18]H. H. Gong, X. H. Chen, Y. Xu, Y. T. Chen, F. F. Ren, B. Liu, S. L. Gu, R. Zhang, and J. D. Ye, IEEE T.. Electr. Dev. 67, 3341 (2020).

[19]Sahadeb Ghosh, Madhusmita Baral, Rajiv Kamparath, S. D. Singh and Tapas Ganguli, Appl. Phys. Lett. 115, 251603 (2019).

[20]X. Lu, Xianda Zhou, Huaxing Jiang, Kar Wei Ng, Zimin Chen, Yanli Pei, Kei May Lau and Gang Wang, IEEE Electr. Dev. L.41, 449 (2020).

[21]Jiaye Zhang, Shaobo Han, Meiyan Cui, Xiangyu Xu, Weiwei Li, Haiwan Xu, Cai Jin, Meng Gu, Lang Chen and Kelvin H. L. Zhang, ACS Appl. Electron. Mater. 2, 456 (2020).

[22]J.D. Hwang and T.H. Ho, Mater. Sci. Semicond. Process. 71, 396 (2017).

[23]D.Y. Jiang, J.M. Qin, X. Wang, S. Gao, Q.C. Liang, J.X. Zhao, Vaccum 86, 1083 (2012),

[24]I. Hotový, D. Búc, ˇS. Haˇsˇcík, O. Nennewitz, Vacuum 50, 41 (1998).

[25]Y. Zhao, H. Wang, F. Yang, Z. Zhen, X. Li, Q. Li and J. Li, Vacuum 151, 163 (2018).

[26]H.L. Lu, G. Scarel, M. Alia, M. Fanciulli, S.J. Ding, D.W. Zhang, Appl. Phys. Lett. 92, 2006 (2008).

[27]H. Sun, S.C. Chen, S.W. Hsu, C.K. Wen, T.H. Chuang, X. Wang, Ceram. Int.43, S369 (2017).

[28]J.L. Yang, Y.S. Lai, J.S. Chen, Thin Solid Films 488, 242 (2005),

[29]S.C. Chen, C.K. Wen, T.Y. Kuo, W.C. Peng, H.C. Lin, Thin Solid Films 572, 51 (2014).

[30]Y. Zhao, H. Wang, C. Wu, Z.F. Shi, F.B. Gao, W.C. Li, G.G. Wu, B.L. Zhang, G.T. Du, Vacuum 103, 14 (2014) .

[31]A. Karpinski, A. Ferrec, M. Richard-Plouet, L. Cattin, M.A. Djouadi, L. Brohan, and P.Y. Jouan, Thin Solid Films 520, 3609 (2012).

[32]A.A. Ahmed, M. Devarajan and N. Afzal,Mater. Sci. Semicond. Process. 63, 137 (2017).

[33]Zhou, Hong, Shifan Zeng, Jincheng Zhang, Zhihong Liu, Qian Feng, Shengrui Xu, Jinfeng Zhang, and Yue Hao, Crystals 11, 1186 (2021).

[34]B.P. Payne, M.C. Biesinger and N.S. McIntyre, J. Electron. Spectroscopy and Rel Phen. 185, 159 (2012).

[35]Hideo Hosono, Toshio Kamiya, State and Role of Hydrogen in Amorphous Oxide Semiconductors, in Amorphous Oxide Semiconductors: IGZO and Related Materials for Display and Memory, 145-157 (John Wiley & Sons, NY 2022).

[36]Michael Stavola, Figen Bekisli, Weikai Yin, Kirby Smithe, W. Beall Fowler, and Lynn A. Boatner, J. Appl. Phys. 115, 012001 (2014).

[37]M.D. McCluskey, M.C. Tarun and S.T. Teklemichael, J. Mat. Res 27, 2190 (2012).

[38]J. E. N. Swallow, J. B. Varley, L. A. H. Jones, J. T. Gibbon, L. F. J. Piper, V. R. Dhanak, and T. D. Veal, APL Mater 7, 022528 (2019).

[39]A. Y. Polyakov, In-Hwan Lee, N. B. Smirnov, E. B. Yakimov, I. V. Shchemerov, A. V. Chernykh, A. I. Kochkova, A. A. Vasilev, F. Ren, P. H. Carey IV, and S. J. Pearton, Appl. Phys. Lett. 115, 032101 (2019).

[40]Xinyi Xia, Jian Sian Li, Chao Ching Chiang, Timothy Jinsoo Yoo, Fan Ren, Honggyu Kim and S.J. Pearton, J. Vac. Sci. Technol A40, 053401 (2022).

[41]E. A. Kraut, R. W. Grant, J. R. Waldrop, and S. P. Kowalczyk, Phys. Rev. Lett., 44, 1620 (1980).

[42]Grzegorz Greczynski and Lars Hultman, J. Appl. Phys. 132, 011101 (2022).

[43]D. C. Hays, B.P. Gila, S. J. Pearton and F. Ren, Appl. Phys. Rev., 021301 (2017).

[44] R.T. Tung, Appl. Phys. Lett, 58, 2821 (1992).

[45]Jian-Sian Li, Chao-Ching Chiang, Xinyi Xia, Fan Ren, and S.J. Pearton, J. Vac. Sci. Technol. A, A 40, 063407 (2022).

[46] Prakash P. Sundaram, Fikadu Alema, Andrei Osinsky, and Steven J. Koester, J. Vac. Sci. Technol. A 40, 043211 (2022).

Journal of Vacuum Science & Technology A

PLEASE CITE THIS ARTICLE AS DOI: 10.1116/6.0002250

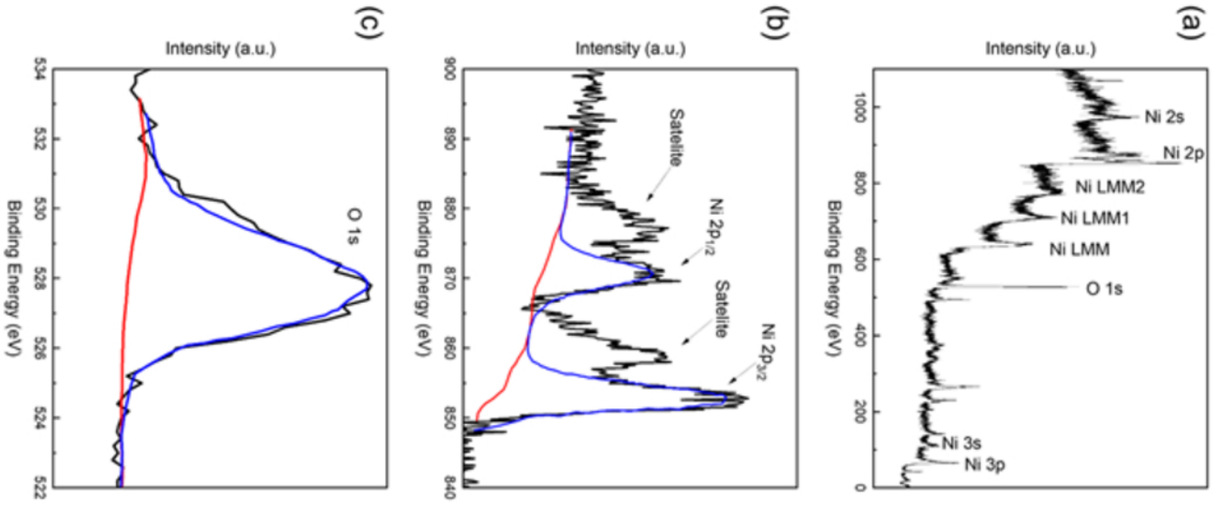

Journal of Vacuum Science & Technology A

PLEASE CITE THIS ARTICLE AS DOI: 10.1116/6.0002250

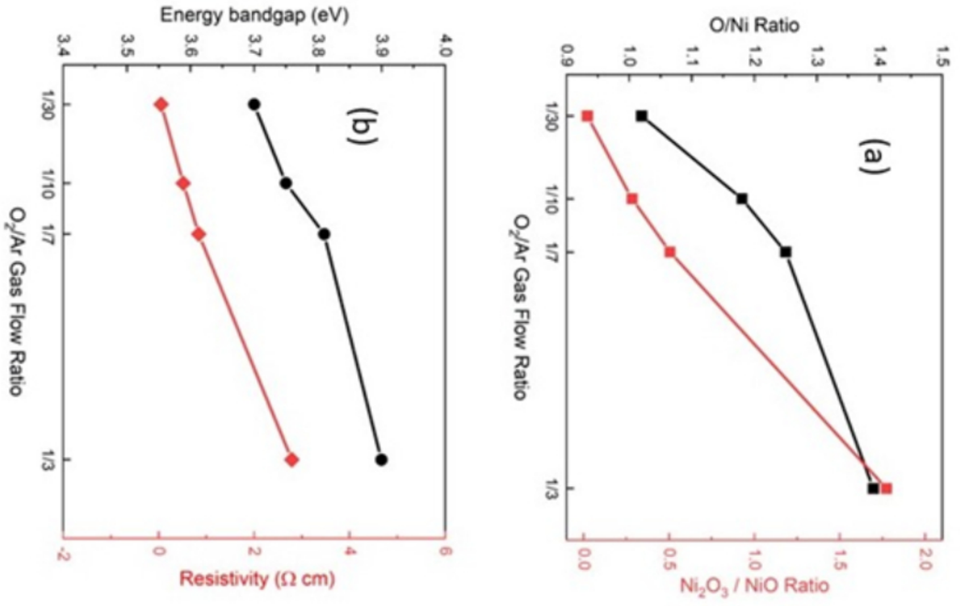

Journal of Vacuum Science & Technology A

PLEASE CITE THIS ARTICLE AS DOI: 10.1116/6.0002250

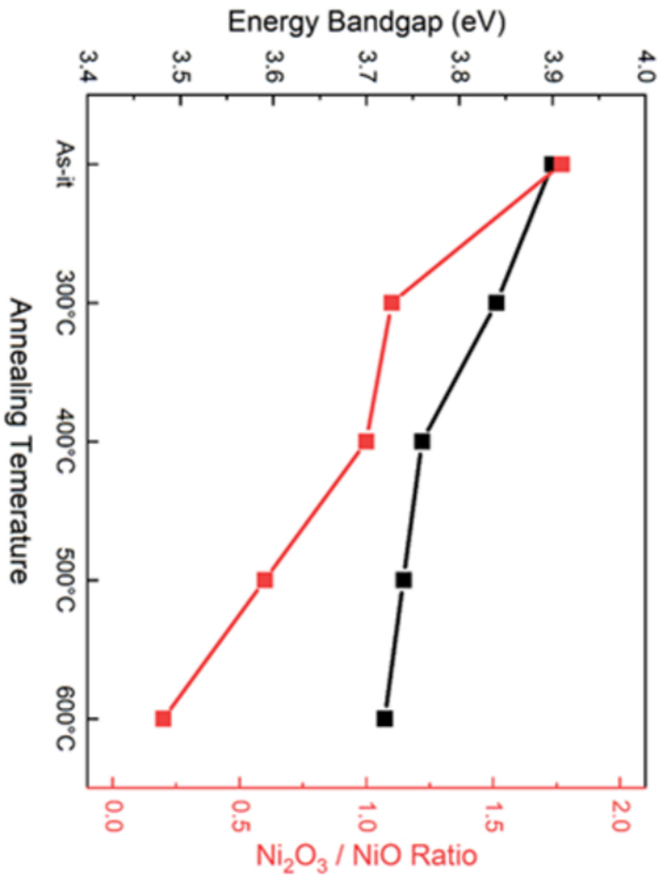

Journal of Vacuum Science & Technology A

ACCEPTED MANUSCRIPT

This is the author's peer reviewed, accepted manuscript. However, the online version of record will be different from this version once it has been copyedited and typeset.
PLEASE CITE THIS ARTICLE AS DOI: 10.1116/6.0002250

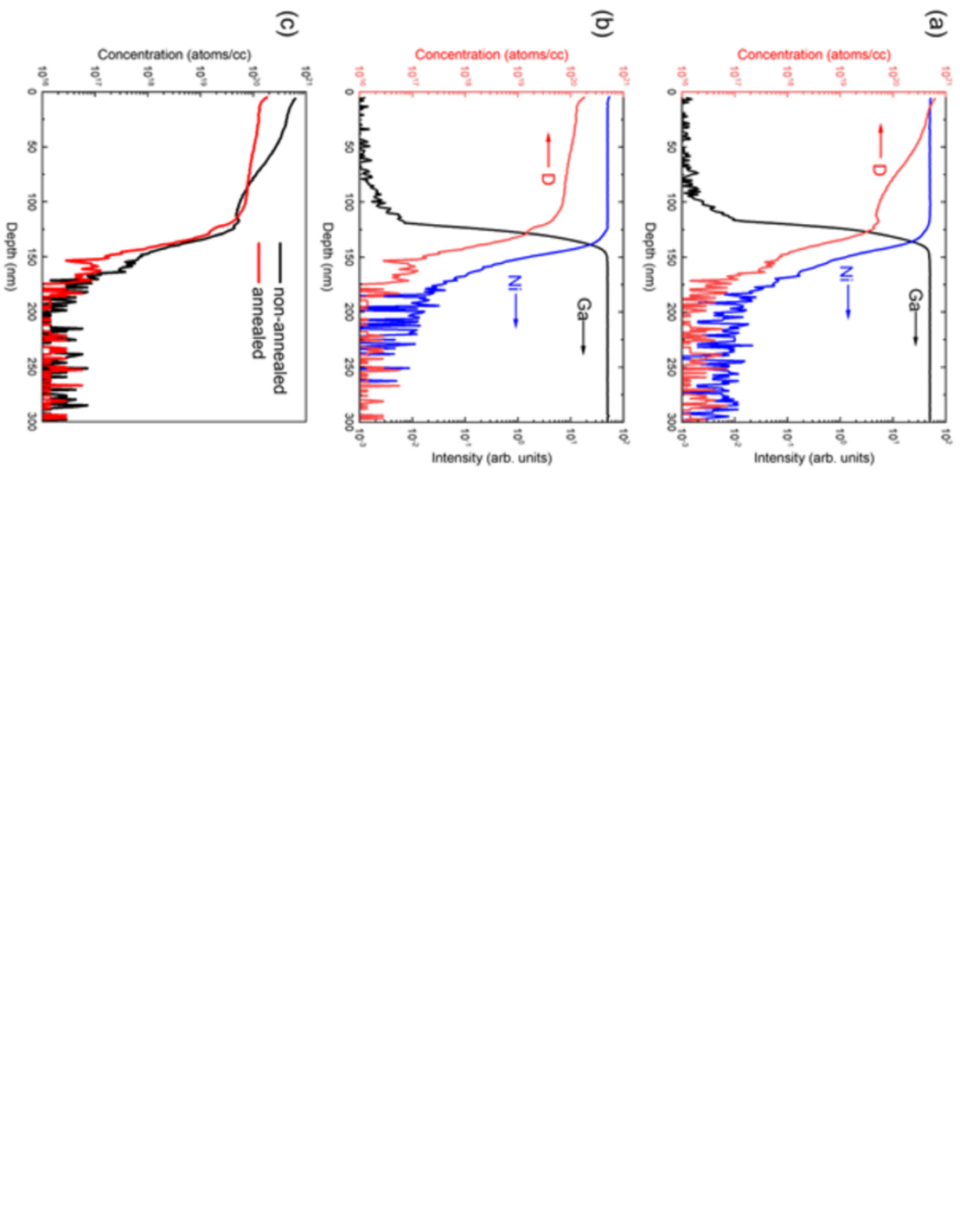

Journal of Vacuum Science & Technology A

PLEASE CITE THIS ARTICLE AS DOI: 10.1116/6.0002250

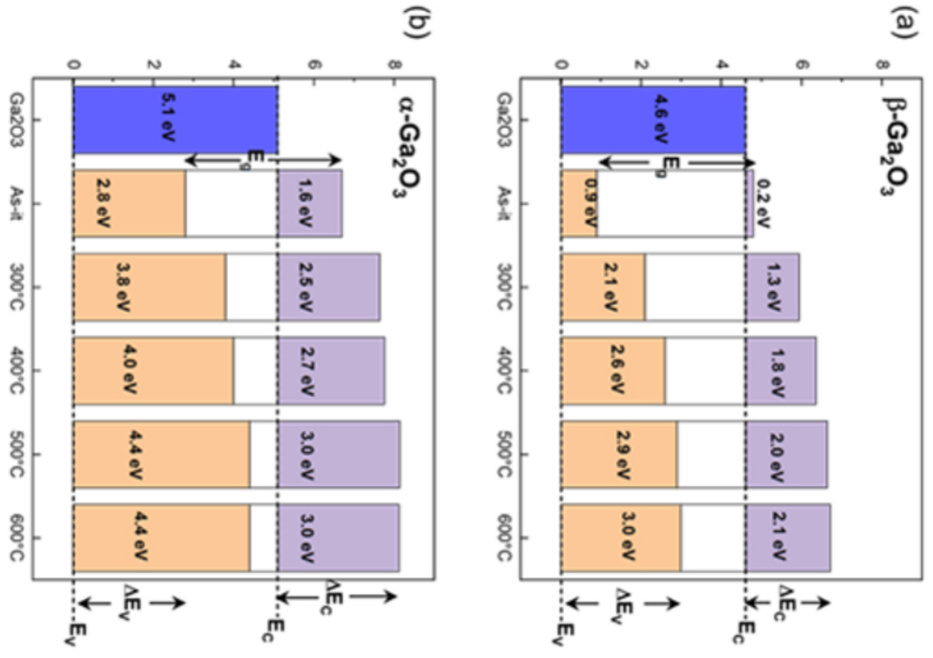

Journal of Vacuum Science & Technology A

PLEASE CITE THIS ARTICLE AS DOI: 10.1116/6.0002250

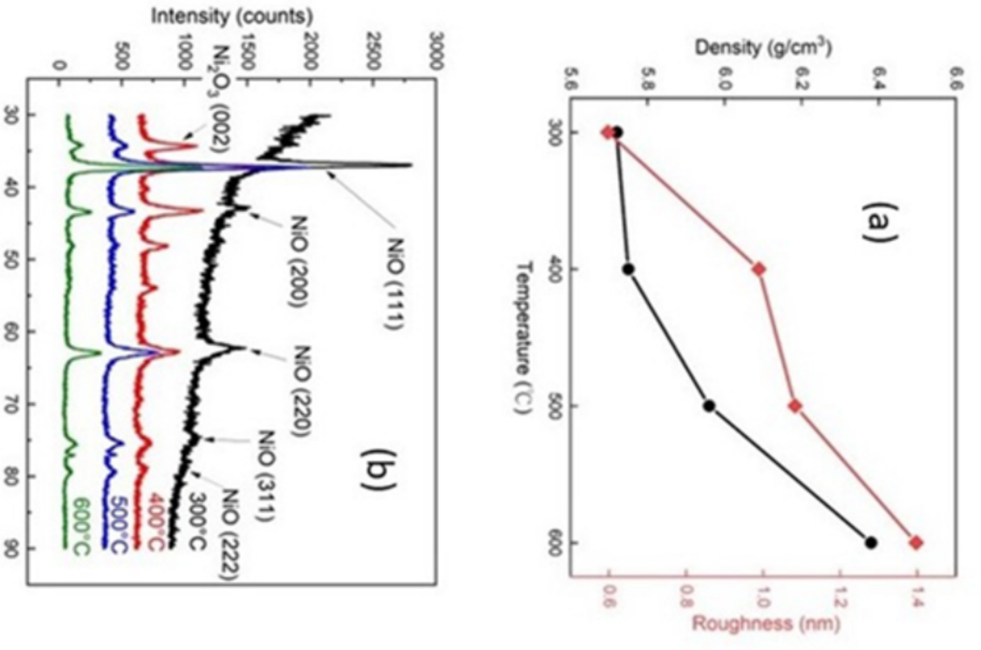

Journal of Vacuum Science & Technology A

PLEASE CITE THIS ARTICLE AS DOI: 10.1116/6.0002250

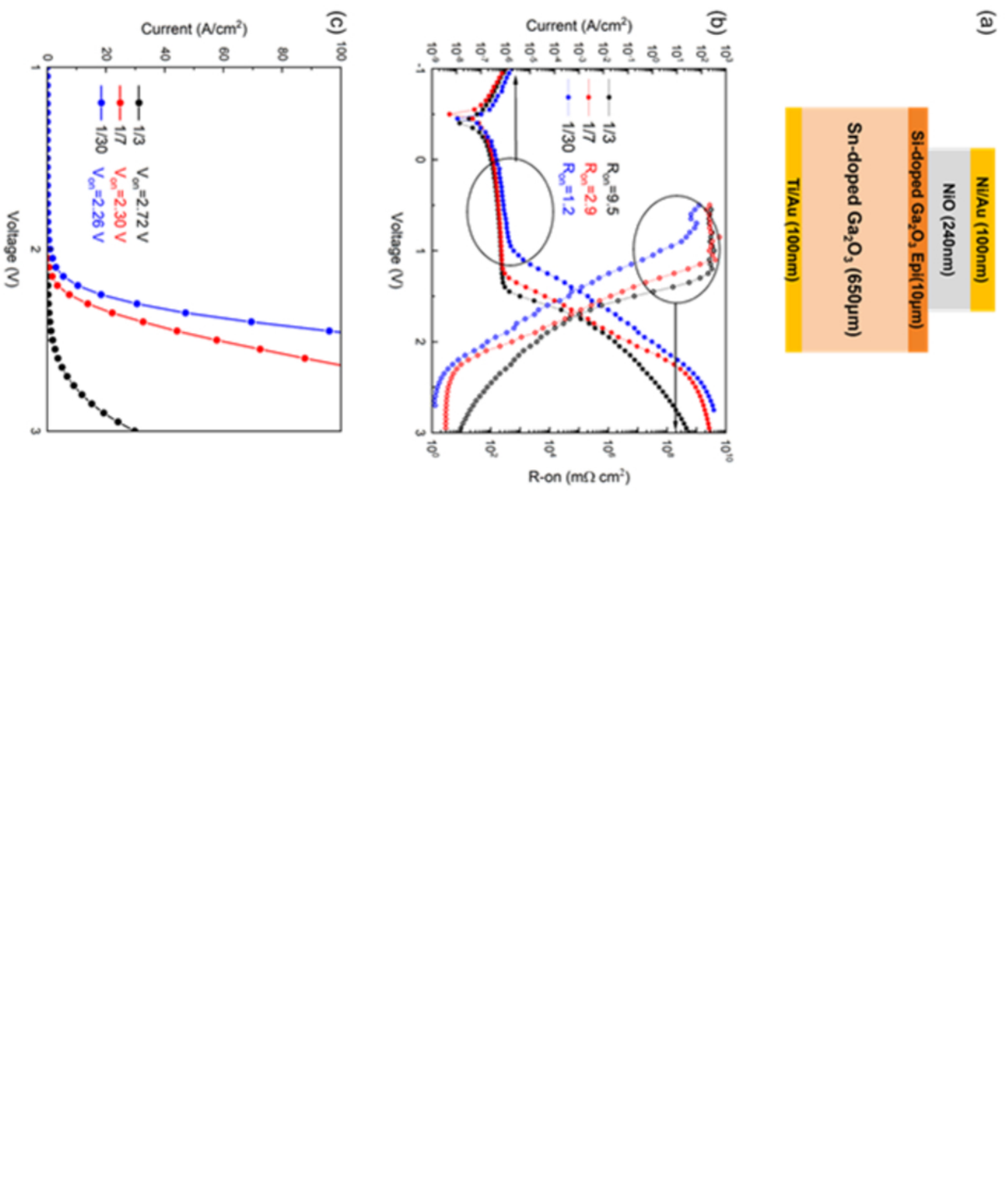

Journal of Vacuum Science & Technology A

PLEASE CITE THIS ARTICLE AS DOI: 10.1116/6.0002250